Uniform Motion Blur in Poissonian Noise: Blur/Noise Trade-off

Giacomo Boracchi and Alessandro Foi

Abstract—In this paper we consider the restoration of images corrupted by both uniform motion blur and Poissonian noise. We formulate an image formation model that explicitly takes into account the length of the blur point-spread function and the noise level as functions of the exposure time. Further, we present an analysis of the achievable restoration performance by showing how the root mean squared error varies with respect to the exposure time. It turns out that the worst situations are represented by either too short or too long exposure times. In between there exists an optimal exposure time that maximizes the restoration performance, balancing the amount of blur and noise in the observation. We justify such result through a mathematical analysis of the signal-to-noise ratio in Fourier domain; this study is then validated by deblurring synthetic data as well as camera raw data.

Index Terms—blur modeling, noise modeling, image restoration, deconvolution, digital camera imaging.

I. INTRODUCTION

This paper concerns restoration from uniform motion blur, which is the blur produced by a convolution against a point-spread function (PSF) that is constant on its straight 1-D support. Uniform motion blur is a simplified description of the blur resulting from some translational motion between camera and scene during the exposure.

Under noisy conditions, inversion of uniform motion blur is particularly challenging due to the patterns of zeros in the Fourier domain. Nevertheless, this type of blur has been the subject of the earliest works on image restoration [1]–[3], mainly because of the simple parametric description of the corresponding PSFs in terms of blur extent and direction. Recently, uniform motion blur has been considered in blind image restoration algorithms [4], [5], in the restoration of pictures containing moving objects [6], and in a study on how the restoration performance varies when several uniform motion blurred images are available [7]. Uniform motion blur seriously affects aerial images, and forward motion compensation (FMC) hardware [8] is typically exploited in order to attenuate the image degradation due to plane or satellite motion. FMC devices are either based on mechanical actuation (e.g., by physically translating the imaging sensor during the exposure time) or on time-delayed integration (i.e. a specialized charged coupled device that, during the exposure, shifts the rows of charged pixels together with the motion): in both cases the exact ground speed and the flight altitude are required. The optical image stabilization methods, nowadays becoming omnipresent in digital cameras, are instead based on accelerometers which as such cannot sense the uniform motion causing the blur. Hence, under many circumstances, uniform motion blur needs to be compensated by means of digital image processing.

Although uniform blur has been often considered in the literature, the blur and noise have been always considered independent whereas in practice they are always linked: e.g., by controlling the exposure time of a digital sensor, one can reduce the noise level at the expense of heavier blur, and vice versa. This paper aims at filling this gap, by introducing an image formation model that describes the interplay between noise, blur, and signal intensity as the exposure

Giacomo Boracchi is with the Dipartimento di Elettronica e Informazione, Politecnico di Milano, Italy

Alessandro Foi is with the Department of Signal Processing, Tampere University of Technology, Finland

time varies. This model is particularly suited for the raw data from digital imaging sensors (see, e.g., [9], [10]). The proposed model allows to evaluate the trade-off between noise and blur, aiming at establishing an optimal exposure time for which the image quality can be maximized by means of a deconvolution algorithm. It turns out that such optimal exposure time is, to a first approximation, independent from the original image (i.e. the underlying image without blur and noise), as images having different content demonstrate similar optimal exposure-time values.

The rest of the paper is organized as follows. Section II introduces the image formation model and shows how the noise level in the observed data varies with the exposure time. In Section III we present an analytical analysis of the best restoration performance achievable by blur inversion in an ideal scenario where the PSF is known. This analysis is consistent with the experimental results given in Section IV. In particular, we show results obtained for synthetically blurred images as well as for raw data from digital camera. Section V concludes the paper presenting some implications of these findings to practical applications.

II. IMAGE FORMATION MODEL

We model an image z_T acquired with an exposure time T as

$$z_T(x) = \kappa \left(u_T(x) + \eta(x) \right), \qquad x \in X, \qquad (1)$$

where $X \subseteq \mathbb{R}^2$ is the sampling grid and $\kappa > 0$ is a factor that can be used for scaling the signal into a usable (limited) dynamic range, thus mimicking the amplification gain in digital sensors (typically, $\kappa \propto T^{-1}$). The two components $u_T(x)$ and $\eta(x)$ are independent random variables distributed as

$$u_T(x) \sim \mathcal{P}\left(\lambda \int_0^T y(x - vt)\, dt \right), \qquad (2)$$
$$\eta(x) \sim \mathcal{N}\left(0, \sigma^2 \right),$$

where $\mathcal{P}$ and $\mathcal{N}$ denote respectively the Poisson and Gaussian distributions, and $\lambda > 0$ is a parameter characterizing the quantum efficiency of the sensor [9]. The function $y : \mathbb{R}^2 \to \mathbb{R}^+$ represents the original image while $v \in \mathbb{R}^2$ identifies the blur direction and velocity. The term η represents a source of noise that is independent from the original image y. In what follows, in order to simplify some derivations, we assume $0 < m \le y \le M < \infty$. This assumption is always satisfied in practical applications.

A. Uniform Blur PSF

The blur is modeled as a linear and shift-invariant operator and, thus, using generalized functions, the argument of the Poisson distribution in (2) can be rewritten as

$$\lambda \int_0^T y(x - vt)dt = \lambda \int_0^T (y \circledast \delta_{vt})(x)dt =$$
$$= \lambda \left(y \circledast \int_0^T \delta_{vt}dt \right)(x) = \lambda(y \circledast h_T)(x), \quad (3)$$

where δ_{vt} denotes the Dirac delta function at $vt \in \mathbb{R}^2$ and $h_T(\cdot) = \int_0^T \delta_{vt}(\cdot)dt$ is the PSF of uniform motion blur. In the simple parametric description of uniform motion blur PSF, the direction and the extent correspond to the direction of v and $L = |vT|$, respectively. This PSF is therefore a line mass supported on the segment vT. In particular, it follows

$$\int_{\mathbb{R}^2} h_T(s)ds = T. \qquad (4)$$

Note that despite PSFs are often assumed to have unit mass, in our model the mass, given by the integral (4), equals the exposure time T: in such a way, we take into account how the signal expectation

varies with respect to the exposure time. The parameter κ in (1) will eventually take care of the normalization. Since we restrict to uniform blur PSF, out-of-focus or blur due to camera optics are neglected as these are time-independent.

B. Noise

Equation (1) can be then rewritten in the following form:

$$z_T(x) = E\{z_T(x)\} + \text{std}\{z_T(x)\}\,\alpha(x), \qquad (5)$$

where $\alpha(x)$ is a random variable with zero mean and unitary variance and overall α is an independent homoskedastic process. The expectation and the standard deviation of our observations are, respectively,

$$E\{z_T(x)\} = \kappa E\{u_T(x)\} =$$
$$= \kappa\lambda\int_0^T y(x-vt)\,dt = \kappa\lambda(y \circledast h_T)(x), \quad x \in X \quad (6)$$

and

$$\text{std}\{z_T(x)\} = \kappa\sqrt{\text{var}\{u_T(x)\} + \text{var}\{\eta(x)\}} =$$
$$= \kappa\sqrt{\lambda(y \circledast h_T)(x) + \sigma^2} = \sqrt{\kappa E\{z_T(x)\} + \kappa^2\sigma^2}. \quad (7)$$

The two terms $u_T - E\{u_T\}$ and η respectively model the signal-dependent noise, inherent to the photon acquisition process, and the signal-independent electric and thermal noises. The latter are approximated as independent of the exposure time and thus, while u_T is influenced by the exposure time, η is not.

C. Observation SNR

Let us now consider how the exposure time influences the signal-to-noise ratio (SNR) between the expectation of the observation (meant as the *signal*) and its noise. Since $h_T > 0$, from (4) we have

$$\inf_{s \in \mathbb{R}^2}\{y(s)\}T \leq (y \circledast h_T)(x) \leq \sup_{s \in \mathbb{R}^2}\{y(s)\}T, \ \forall x \in X. \quad (8)$$

From the above inequality and from (7), it follows $\forall x \in X$

$$\kappa\sqrt{\lambda T \inf_{s \in \mathbb{R}^2}\{y(s)\} + \sigma^2} \leq$$
$$\leq \text{std}\{z_T(x)\} \leq$$
$$\leq \kappa\sqrt{\lambda T \sup_{s \in \mathbb{R}^2}\{y(s)\} + \sigma^2}. \quad (9)$$

Thus, for T large enough we have $\text{std}\{z_T(x)\} \asymp \kappa\sqrt{\lambda T}$, where the $\asymp$ symbol indicates that the ratio between the two terms is bounded from above and from below by two strictly positive constants. Similarly, one may derive from (6) that $E\{z_T(x)\} \asymp \kappa\lambda T$. This leads to an asymptotic expression for long exposure times of $\text{SNR}(z_T(x))$, the signal-to-noise ratio of z_T at $x \in X$:

$$\text{SNR}(z_T(x)) = \frac{E\{z_T(x)\}}{\text{std}\{z_T(x)\}} \asymp \sqrt{\lambda T} \underset{T \to +\infty}{\longrightarrow} +\infty. \quad (10)$$

On the contrary, for T small enough we have that $\text{std}\{z_T(x)\} \asymp \kappa\sqrt{\lambda T + \sigma^2}$, and $E\{z_T(x)\} \asymp \kappa\lambda T$. Then, the corresponding asymptotic expression of $\text{SNR}(z_T(x))$, for short exposure times is

$$\text{SNR}(z_T(x)) = \frac{E\{z_T(x)\}}{\text{std}\{z_T(x)\}} \asymp T^\beta \underset{T \to 0}{\longrightarrow} 0, \quad (11)$$

with $\beta = 0.5$ when $\sigma = 0$, and $\beta = 1$ otherwise.

Note however that because of the blur, the increase of the $\text{SNR}(z_T(x))$ in (10) does not necessarily correspond to an observation that can lead to a better restoration. Such a correspondence holds when the blur effects do not increase with the exposure: for the uniform blur this happens, for example, when y is constant along
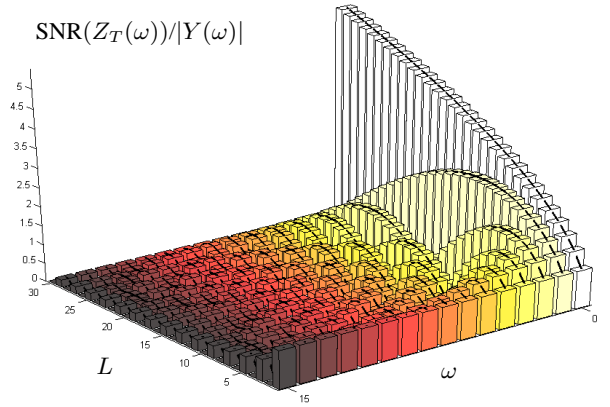

Fig. 1. The factor enclosed in square brackets of Equation (14), when $\sigma = 0$ and $\lambda = 1$. The plot illustrates how the normalized signal-to-noise ratio $\text{SNR}(Z_T(\omega))/|Y(\omega)|$ on each frequency ω varies as a function of the PSF extent $L = 1,\ldots,30$, and thus as a function of the exposure time T. Only on the DC component the SNR increases with the exposure time while, on the other frequencies $\omega \neq 0$, the upper bound of the SNR decreases.

the PSF direction, or when v is zero. Only for such exceptional cases the $\text{SNR}(z_T)$ can be a meaningful indicator of the restoration quality. Otherwise, while $E\{z_T(x)\}$ increases and $\text{std}\{z_T(x)\}$ decreases with the exposure time, the blur extent increases, making the restoration more challenging.

In order to clarify the interplay between blur and noise with the increase of the exposure time, we now reformulate the above inequalities in Fourier domain. In what follows, for the sake of simplicity, we will consider discrete domain variables, ignoring possible aliasing effects in the convolutions.

III. FOURIER DOMAIN ANALYSIS

The Fourier transform Z_T of the observation z_T can be expressed thanks to (5)-(7) as

$$Z_T(\omega) = \lambda\kappa Y(\omega)H_T(\omega) + S_T(\omega)\Theta(\omega), \quad (12)$$

where $\Theta(\omega)$ is a complex valued random variable with unit variance and zero mean, Y and H_T are the Fourier transforms of y and h_T, respectively, and

$$S_T^2(\omega) = \sum_{x \in X}\text{var}\{z_T(x)\} = \kappa^2\sum_{x \in X}\left(\lambda(y \circledast h_T)(x) + \sigma^2\right). \quad (13)$$

This equality follows from the independence of α in (5), and from the fact that the basis elements of the Fourier transform take their values on the unit circle in the complex plane. On similar grounds, we remark that Θ is not an independent and identically distributed process.

The SNR on each frequency allows us to speculate on the effects of both blur and noise in our observation. Let $\text{SNR}(Z_T(\omega))$ be the computed SNR for the frequency ω of our observation, i.e.

$$\text{SNR}(Z_T(\omega)) = |Y(\omega)|\left[\frac{\lambda|H_T(\omega)|}{\sqrt{\sum_{x \in X}\lambda(y \circledast h_T)(x) + (\#X)\sigma^2}}\right], \quad (14)$$

where $(\#X)$ stands for the cardinality of X.

Considerations similar to those leading to inequalities (9) give the following upper bound for the $\text{SNR}(Z_T(\omega))$:

$$\text{SNR}(Z_T(\omega)) \leq |Y(\omega)|\frac{\lambda|H_T(\omega)|}{\sqrt{(\#X)(\lambda cT + \sigma^2)}}, \quad (15)$$

$c > 0$ being a suitable constant.

As discussed in Section II-A, we have that h_T is a line mass uniform over its 1-D segment support, whose length is proportional

Fig. 2. Experiments on synthetically generated observation: the top row shows an observation detail and the PSF used for generating each blurred noisy image. These observations were generated with $\kappa = 1$, $\lambda = 24000$, $\sigma = 0$ and exposure times $T = 0.005, 0.0188, 0.0707, 0.2659, 1$, respectively. The bottom row shows the restored images: the RMSEs (computed on the whole image) are $7.4671, 5.9970, 4.7432, 6.3724, 8.9060$, respectively. Note that all the observations and the PSFs have been rescaled for visualization purpose.

to the exposure time T. Without loss of generality, we assume that the support of h_T is horizontal: this allows us to carry out the analysis of the SNR in frequency domain by considering 1-D Fourier transform (the 2-D Fourier transform of h_T is constant along lines $\omega_2 = const$). Let then H_T be the 1-D Fourier transform of h_T: apart from the DC component ($\omega = 0$), $H_T(\omega)$, $\omega \neq 0$ is a *sinc* function that satisfies $|H_T(\omega)| \leq 1/|\omega|$. Therefore inequality (15) becomes

$$\text{SNR}\left(Z_T(\omega)\right) \leq \frac{\lambda |Y(\omega)|}{|\omega| \sqrt{(\#X)(\lambda c T + \sigma^2)}}, \quad \omega \neq 0. \quad (16)$$

In other words, for any fixed frequency $\omega \neq 0$, the upper bounds for SNR $(Z_T(\omega))$, decrease like $T^{-0.5}$.

Figure 1 shows how the factor in square brackets in (14) varies with the extent L, and thus with the exposure time T. The considered PSFs have constant value 1 on their support of length $L = 1, \ldots, 30$ pixels. In this way, Figure 1 illustrates how, for any original image y, the SNR on each frequency of the observation Z is scaled when the exposure time varies. The SNR of the DC component, SNR $(Z_T(0))$, increases monotonically with respect to the exposure time, while on all the other frequencies ($\omega \neq 0$), SNR $(Z_T(\omega))$ shows a sinusoidal behavior with respect to the exposure time. Equation (16) implies that the local maxima of these sinusoids are decreasing with the exposure time T, and that such decay is faster the higher is the frequency.

A. Blur and Inversion

Equation (16) gives a quantitave estimate of the poor conditioning resulting from rectilinear blur as the exposure time varies. Regardless of the particular technique utilized for recovering y out of z, the inversion of the blur shall aim at scaling the attenuated spectral components $Z_T(\omega)$ back to $Y(\omega)$. Diagonal inverses, such as the pseudoinverse or a regularized inverse, operate by frequency-wise multiplication of each $Z_T(\omega)$ by an appropriate scaling factor, and in these cases the SNR on each frequency of the restored image varies proportionally to the term in squared brackets from (14). Effective deblurring techniques are instead essentially *non-diagonal* operators[1], as they exploit the existing structural correlations in the underlying image y to restrain the noise. Nevertheless, also in this case, the

---

[1] the non-diagonality is meant with respect to the Fourier spectrum, regardless of the particular domain in which the deblurring technique operates.

SNR of non-DC components of the restore image will, as T grows, necessarily decrease unless more and more correlations are exploited as a result of some kind of (adaptive) filtering. However, because the correlations in y are fixed, and because the $T^{-0.5}$ rate for (16) holds for all $\omega \neq 0$, we can conclude that this particular rate is generally valid for any deblurring algorithm for T large enough. Thus, the SNR after the blur inversion follows, for each ω, a limiting trend like the one shown in Figure 1, which tells us that for an increasing exposure time one will eventually be able to recover only the mean values of the image along lines parallel to the blur direction.

B. Optimal Exposure Time

From the equations derived so far we can conclude that, in case of uniform blur, increasing the exposure time may not result in observations that are easier to restore, as the conditioning of the blur operator may worsen. In particular, for each individual non-zero frequency, the corresponding SNR is inevitably maximized at a finite exposure time. In principle, this does not have any direct implication on the overall quality of the restored image, because such exposure times might not be the same for every frequency and, moreover, on each frequency SNR$(Z_T(\omega))$ depends on the image spectrum $|Y(\omega)|$, as shown in (14). Consider, for example, the trivial cases where y is flat or contains only stripes perfectly aligned with the PSF: the longer is the exposure, the less the noise affects the resulting image, while instead the blur leaves the image unchanged. However, except from these cases and all other situations where the AC terms in the image spectrum are dominated by the DC term alone, it is natural to expect the overall quality to eventually decrease, as the exposure time goes to infinity. Thus, it appears that there exists a finite *optimal exposure time* that, balancing the blur/noise trade-off, maximizes the quality of the restored image. The following experiments aim at establishing the existence of this optimal exposure time within a concrete deblurring application and at assessing how its value is affected by the image content and noise parameters.

IV. EXPERIMENTS

In this section, we show how the restoration performance varies with the exposure time, first by considering a dataset of synthetically
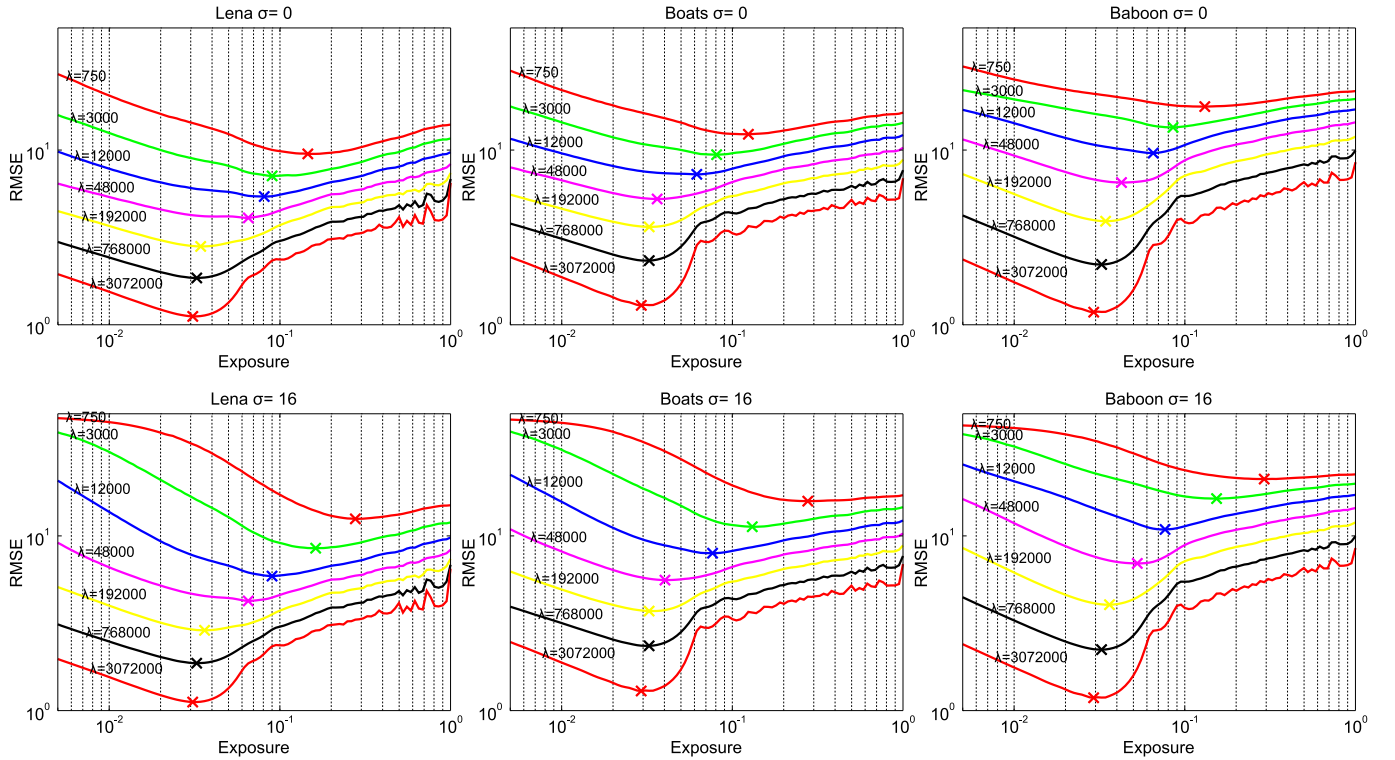
Fig. 3. Ideal restoration performance (the blur PSF is known and an oracle regularization parameter $\varepsilon^\star$ has been used): tests on *Lena, Boats* and *Baboon*. Each plot shows the RMSE when restoring observations generated with varying exposure times from a fixed test image. Different curves in each plot represent the RMSE for different values of λ, when $\sigma = 0$ and $\sigma = 16$. A cross marks the minimum of each curve, and represents the optimal exposure time and the corresponding restoration performance.

blurred and noisy observation, and second by restoring blurred and noisy raw-data images acquired with a digital camera.

The image restoration algorithm used is the LPA-ICI deconvolution for signal-dependent noise[2] [11], [12]. This algorithm is based on a nonparametric Poisson ML modeling and it couples the Tichonov regularized inverse

$$\hat{Y}_{T,\varepsilon}^{RI} = Z_T \frac{\overline{H_T}}{|H_T|^2 + S_T^2 \varepsilon^2} \qquad (17)$$

with adaptive anisotropic filtering. This filtering is realized in spatial domain, using directional polynomial-smoothing kernels $g_{\theta_i, h^+(\theta_i)}$ having pointwise-adaptive support-size $h^+(\theta_i)$ along the different directions θ_i: the final restored image $\hat{y}$ is computed as

$$\hat{y}(x) = \sum_{\theta_i} \beta\left(x, h^+(\theta_i), \theta_i\right) \int \hat{y}_{T,\varepsilon}^{RI}(\xi)\, g_{\theta_i, h^+(\theta_i)}(x-\xi)\, d\xi, x \in X,$$

where $\hat{y}_{T,\varepsilon}^{RI}$ is the inverse Fourier transform of $\hat{Y}_{T,\varepsilon}^{RI}$ (17), and the convex weights $\beta\left(x, h^+(\theta_i), \theta_i\right)$ are used to combine the directional estimates into an anisotropic one. For details we refer the reader to [13] and especially to [12].

As criterion, we utilize the root mean squared error (RMSE) computed between the rescaled $\hat{y}$ and the original image y,

$$\text{RMSE}(\hat{y}, y) = 255 \sqrt{\frac{1}{\#X} \sum_{x \in X} \left(\frac{1}{\kappa\lambda} \hat{y}(x) - y(x)\right)^2}.$$

We assume that the PSF h_T is exactly known; moreover, an oracle regularization parameter $\varepsilon^\star$ is selected for each observation by minimizing the RMSE. The minimization has been carried out using the Nelder-Mead algorithm [14], [15]. Although these assumptions are rarely met in practice, they allow to investigate how the potential restoration performance varies with the exposure time: for this reason,

in the sequel, this RMSE is referred to as the *ideal restoration performance*.

A. Deblurring of Synthetic Data

We synthetically generate several blurred and noisy observations according to Equation (1) using five standard 512×512 grayscale test images (*Lena, Hill, Boats, Baboon, Man*), by considering 100 exposure times exponentially distributed between $T_1 = 0.005$ and $T_{100} = 1$. The test images are normalized so that black and white correspond to 0 and 1, respectively. We restrict to horizontal uniform blur PSFs, generated using subpixel linear interpolation. The PSF supports range from 2 (at T_1) to 34 (at T_{100}) pixels, depending on the exposure time. The top row of Figure 2 shows some details taken from some of the observations generated from *Lena* ($\kappa = 1$, $\lambda = 24000$, $\sigma = 0$, and exposure times $T \in \{0.005, 0.0188, 0.0707, 0.2659, 1\}$), with the corresponding PSFs depicted in the top-left corner, while the bottom row shows the corresponding restored images: their RMSE are, respectively, 7.47, 6.00, 4.74, 6.37, 8.91.

An extensive simulation is made to evaluate the restoration performance under several values of λ (ranging from 750 to 3072000) and σ (ranging from 0 to 32). We fixed $\kappa = 1$, as this scaling factor bears no effect on the result. The plots of Figures 3-4 show the RMSE of the restored image when assuming perfectly known PSF and oracle regularization parameters for each exposure time. In order to reduce the influence of the discretization of PSFs on the image grid, the reported values are, for each exposure time, the averages of the RMSEs obtained after restoring 10 different observations generated by subpixel shifting the PSF of $0.1 \times \{0, 1, \ldots, 9\}$ pixels. Figure 3 shows the results for three different test images for $\sigma = 0$ and $\sigma = 16$, while Figures 3 and 4 show the results averaged over the five considered test images images for all considered λ and σ values.

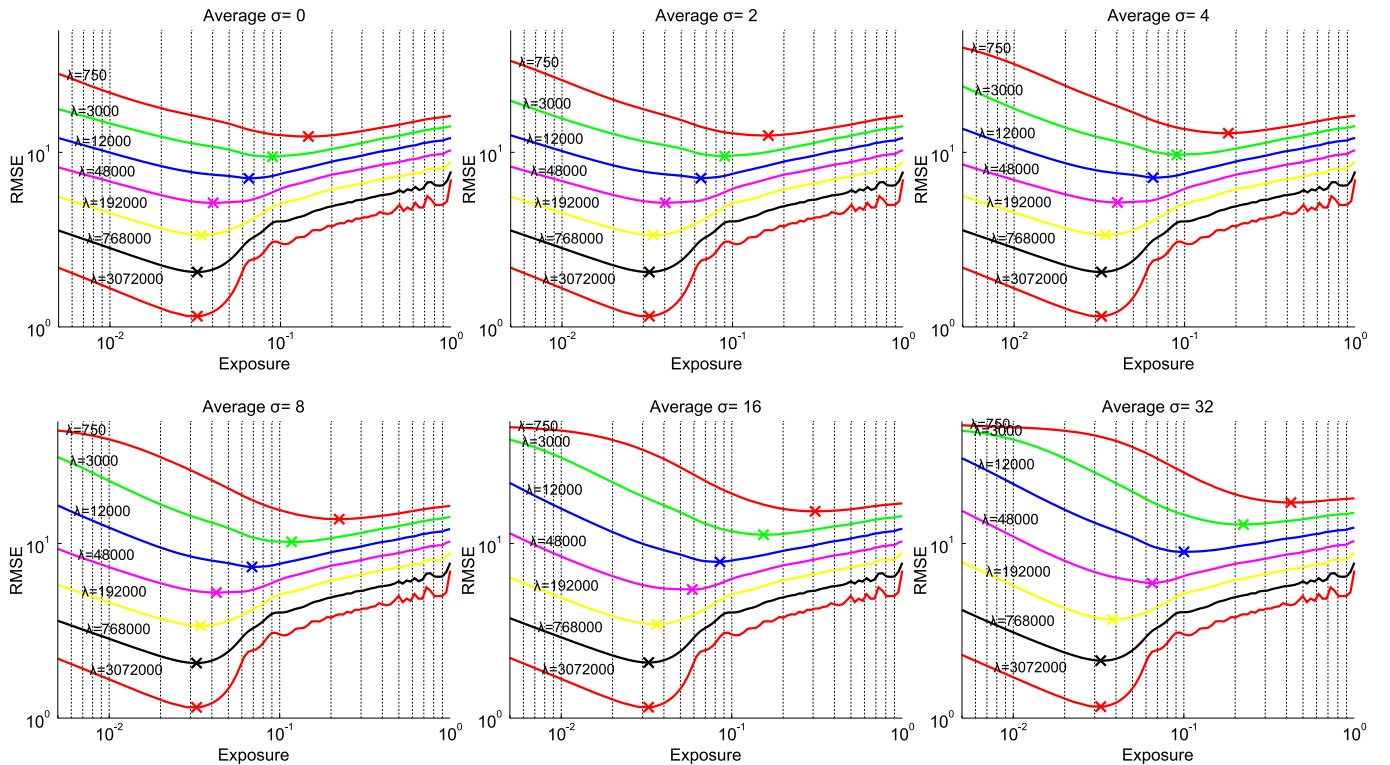---

[2]Available at http://www.cs.tut.fi/~lasip/ .

Fig. 4. Ideal restoration performance (the blur PSF is known and an oracle regularization parameter $\varepsilon^\star$ has been used): the average over the 5 test images. Different curves in each plot represent the average of the RMSE when restoring observations generated with varying exposure times from the 5 test images, as λ varies. Each plot shows the restoration performance when $\sigma = 0, 2, 4, 8, 16, 32$, respectively. The restoration has been performed assuming known PSF and using an oracle regularization parameter $\varepsilon^\star$. A cross marks the minimum of each curve, and represents the optimal exposure time and the corresponding restoration performance.

B. Deblurring of Camera Raw Data

In order to ensure uniform motion blur, we acquired a sequence of pictures in front of a monitor running a short movie containing the *Lena* image progressively translated. A still image of *Lena* was also shown, in order to provide a ground-truth image for measuring the restoration performance. We processed one of the green subchannels of the Bayer raw data. The size of *Lena* imaged in this way was 408×408 pixels. A marker moving together with the image was used as an aid for the estimation of the PSFs, which was obtained via parametric fitting, first on the image of the blurred marker (as initialization), and then through the minimization of the RMSE. Images have been acquired with a Canon EOS 400D 10-Mpixel camera fixed on a tripod: the parallelism between the monitor and the imaging sensor was ensured by controlling that the imaged windows containing the video and the still image were rectangular. We acquired 8 blurred images by changing the camera exposure and ISO parameter as listed in Table I, while all other camera parameters where fixed. The pedestal in the raw data had been subtracted prior to processing, ensuring a linear response of the sensor, while the noise model parameters λ and σ were estimated using the algorithm [9] and are given in Table I. After processing, the image intensities were rescaled adaptively, in order to have all images in the same range. The obtained RMSE results are given in Table I[3], while Figure 5 shows some details

[3]In the table, we list two pairs of values: T and $\hat{\lambda}$ and $\hat{T}$ and λ. T are the exposure times manually selected on the camera and $\hat{\lambda}$ are estimated assuming these values exact. However, according to (2), λ should have a unique value characteristic of the sensor. Hence, λ can be set equal to a fixed value (roughly equal to the median of the $\hat{\lambda}$ values) and $\hat{T}$ are the exposure times derived from this constant λ. By comparing these values with the extents $\hat{L}$ measured from the fitted PSF, one can observe that $\hat{T}$ are slightly more consistent exposure values than T are. We note that the extent $\hat{L}$ estimated for the first image is a clear underestimate of the PSF length, due to the inability of accurately determining the length of a PSF shorter than a pixel.

of the observations together with the estimated PSFs (top row) and the corresponding restored images (bottom row).

C. Discussion

The plots in Figures 3 and 4 show that the behavior of the RMSE with respect to the exposure time is consistent with the equations derived in Sections III and with the trend of the SNR in Fourier domain shown in Figure 1. In particular, the RMSE curves show that the optimal exposure time exists and that after this moment the RMSE eventually increases. Moreover, the oscillations that appear in all plots for large values of λT reflect the oscillatory behavior of the SNR shown in Figure 1. These are not seen unless λT is large enough, because the regularization term in (17) eventually dampens the role of H_T in the deblurring. Note that because of the oracle regularization, the deblurred estimate is in practice never worse than a flat image equal to the mean value of the image, which bounds the RMSE to $255\sqrt{\frac{1}{\#X}\sum_{x \in X}\left(y\left(x\right) - \frac{1}{\#X}\left(\sum_{s \in X} y\left(s\right)\right)\right)^2}$. For this reason, the rate predicted by (11) is never realized and one can observe the effect of oracle regularization in Figure 4 when $\sigma = 32$ and $\lambda = 750$.

Most importantly, the plots show that the optimal exposure time is essentially determined by the λ and σ parameters, whereas the influence of the particular image to be restored is negligible, at least when images are drawn from the same class (in our experiments we have been processing natural test images). Thus, the optimal exposure times found from the plots in Figure 4 can be used for any of the images leading to RMSE results practically identical to the optimal ones. We emphasize that even though our test images are indeed taken from the same class of natural images, they nevertheless portray significant variations in the image content, also in terms of spectral features (e.g., among *Lena, Boat,* and *Baboon*).

Fig. 5. Experiments on camera raw data: raw data images #1,2,3,5,8 with the estimated PSF (top row) and restored images (bottom row). Acquisition parameters and restoration performance are given in Table I. Images have been rescaled for visualization purposes.

TABLE I
RAW-DATA IMAGES: PARAMETERS (SEE TEXT) AND RMSE RESULT AFTER DEBLURRING.

image #	ISO	T (s)	$\hat{T}$ (s)	$\hat{\lambda}$	λ	$\hat{\sigma}$	$\hat{\kappa}$	$\hat{L}$ (pixels)	RMSE
1	1600	1/30	0.033	2984	3000	5.08	1.005×10^{-2}	0.07	8.73
2	1600	1/15	0.067	3020	3000	5.31	4.967×10^{-3}	0.97	5.24
3	1600	1/8	0.134	3210	3000	5.02	2.492×10^{-3}	2.05	4.21
4	800	1/4	0.263	3156	3000	5.91	1.267×10^{-3}	3.88	4.50
5	400	1/2	0.503	3019	3000	7.79	6.625×10^{-4}	6.97	5.93
6	200	1	0.964	2893	3000	10.68	3.456×10^{-4}	14.43	8.43
7	100	2	1.867	2802	3000	18.37	1.784×10^{-4}	26.04	15.22
8	100	2.5	2.23	2674	3000	16.70	1.496×10^{-4}	33.90	20.09

Experiments reported in Figure 5 and in Table I show that the results on camera raw data are consistent with the results obtained on synthetic data.

V. CONCLUDING REMARKS

We presented an image formation model where both the blur due to camera motion and the sensor noise are defined as functions of the exposure time. This model can be directly generalized to arbitrary motion PSFs, and it is thus suited for describing very general acquisition paradigms including the recently proposed approaches based on blurred/noisy image pairs [16], [17], as it offers a unified description of both long-exposure and short-exposure images.

We have shown that in case of uniform blur, increasing the exposure time leads to an improvement of the SNR of the observed blurred and noisy image, but, even in ideal conditions (where the PSF is perfectly known and an oracle regularization term is given), this does not imply an improvement of the restoration performance. On the contrary, our study highlights that there is a finite optimal exposure time which maximizes the restoration performance, balancing the blur/noise trade-off in the observation. According to experiments on both synthetically generated observation and on camera raw data, the estimated optimal exposure times correspond to observations that are corrupted by noise levels that are far form being negligible. Thus, at least in case of uniform motion blur, explicitly handling the noise (even in long-exposure images) becomes a mandatory issue for algorithms that rely on observations acquired with varying exposure times.

Our ongoing research generalizes the presented analysis to random-motion PSFs to investigate the blur/noise trade-off for a wider class of camera motions.

REFERENCES

[1] D. Slepian, "Restoration of photographs blurred by image motion," Bell Syst. Tech., Tech. Rep., 1967, j.46, 23532362.
[2] S. C. Som, "Analysis of the effect of linear smear on photographic images," *J. Opt. Soc. Am.*, vol. 61, no. 7, pp. 859–864, 1971. [Online]. Available: http://www.opticsinfobase.org/abstract.cfm?URI=josa-61-7-859
[3] T. Cannon, "Blind deconvolution of spatially invariant image blurs with phase," *IEEE Trans. Acoustics Speech Signal Process.*, vol. 24, no. 1, pp. 58–63, February 1975.
[4] Y. Yitzhaky, R. Milberg, S. Yohaev, and N. S. Kopeika, "Comparison of direct blind deconvolution methods for motion-blurred images," *Applied Optics*, vol. 38, pp. 4325–4332, Jul. 1999.
[5] A. Rav-Acha and S. Peleg, "Restoration of multiple images with motion blur in different directions," in *Applications of Computer Vision, 2000, Fifth IEEE Workshop on*, 2000, pp. 22–28.
[6] A. Levin, "Blind motion deblurring using image statistics," in *Advances in Neural Information Processing Systems 19*, B. Schölkopf, J. Platt, and T. Hoffman, Eds. Cambridge, MA: MIT Press, 2007. [Online]. Available: http://people.csail.mit.edu/alevin/papers/levin-deblurring-nips06.pdf

[7] A. Rav-Acha and S. Peleg, "Two motion-blurred images are better than one," *Pattern Recogn. Lett.*, vol. 26, no. 3, pp. 311–317, 2005.

[8] R. Pacey and P. Fricker, "Forward motion compensation (FMC) - is it the same in the digital imaging world?" *Photogrammetric Engineering & Remote Sensing*, vol. 71(11), pp. 1241–1242, 2005.

[9] A. Foi, M. Trimeche, V. Katkovnik, and K. Egiazarian, "Practical Poissonian-Gaussian noise modeling and fitting for single-image raw-data," *IEEE Trans. Image Process.*, vol. 17, no. 10, pp. 1737–1754, Oct. 2008.

[10] A. Foi, S. Alenius, V. Katkovnik, and K. Egiazarian, "Noise measurement for raw-data of digital imaging sensors by automatic segmentation of nonuniform targets," *IEEE Sensors Journal*, vol. 7, no. 10, pp. 1456–1461, Oct. 2007.

[11] A. Foi, S. Alenius, M. Trimeche, V. Katkovnik, and K. Egiazarian, "A spatially adaptive Poissonian image deblurring," in *Proc. IEEE Int. Conf. Image Process.*, Genova, Italy, September 2005, pp. 925–928.

[12] V. Katkovnik, K. Egiazarian, and J. Astola, *Local Approximation Techniques in Signal and Image Processing*. SPIE Press, 2006, vol. PM157.

[13] ——, "A spatially adaptive nonparametric regression image deblurring," *IEEE Trans. Image Process.*, vol. 14, no. 10, pp. 1469–1478, October 2005.

[14] J. C. Lagarias, J. A. Reeds, M. H. Wright, and P. E. Wright, "Convergence properties of the Nelder–Mead simplex method in low dimensions," *SIAM J. Optimization*, vol. 9, no. 1, pp. 112–147, 1998.

[15] J. A. Nelder and R. Mead, "A simplex method for function minimization," *The Computer Journal*, vol. 7, pp. 308–313, 1965.

[16] M. Tico and M. Vehviläinen, "Estimation of motion blur point spread function from differently exposed image frames," in *Proc. EUSIPCO 2006*, 2006.

[17] L. Yuan, J. Sun, L. Quan, and H.-Y. Shum, "Image deblurring with blurred/noisy image pairs," *ACM Trans. Graph.*, vol. 26, no. 3, p. 1, 2007.